

## Quantum Anomalous Hall Effect with Higher Plateaus

Jing Wang, Biao Lian, Haijun Zhang, Yong Xu, and Shou-Cheng Zhang

*Department of Physics, McCullough Building, Stanford University, Stanford, California 94305-4045, USA*

(Received 24 May 2013; published 24 September 2013)

The quantum anomalous Hall (QAH) effect in magnetic topological insulators is driven by the combination of spontaneous magnetic moments and spin-orbit coupling. Its recent experimental discovery raises the question if higher plateaus can also be realized. Here, we present a general theory for a QAH effect with higher Chern numbers and show by first-principles calculations that a thin film magnetic topological insulator of Cr-doped  $\text{Bi}_2(\text{Se}, \text{Te})_3$  is a candidate for the  $C = 2$  QAH insulator. Remarkably, whereas a higher magnetic field leads to lower Hall conductance plateaus in the integer quantum Hall effect, a higher magnetic moment leads to higher Hall conductance plateaus in the QAH effect.

DOI: [10.1103/PhysRevLett.111.136801](https://doi.org/10.1103/PhysRevLett.111.136801)

PACS numbers: 73.43.-f, 73.20.-r, 75.50.Pp, 85.75.-d

The topological phases of two-dimensional (2D) insulators with broken time reversal symmetry are characterized by the first Chern number [1], which takes integer values in the integer quantum Hall effect (IQHE). In the IQHE, the electronic states of the 2D electron system form Landau levels under strong external magnetic fields, and the Hall resistance is quantized into  $h/Ce^2$  plateaus [2] contributed by dissipationless chiral states at sample edges [3] (where  $h$  is Planck's constant,  $e$  is the charge of an electron, and  $C$  is the Chern number). In principle, the quantum Hall effect can exist without the external magnetic field and the associated Landau levels [4]; however, the Haldane model [4] with circulating currents on a honeycomb lattice is not easy to implement experimentally. In a quantum anomalous Hall (QAH) insulator, theoretically proposed for magnetic topological insulators (TIs) [5–10], the ferromagnetic (FM) ordering and spin-orbit coupling (SOC) are sufficiently strong that they can give rise to a topologically nontrivial phase with a finite Chern number. Also, the QAH states have been predicted to exist in transition metal oxide heterostructures [11–16]. Recently, the QAH effect has been experimentally discovered in magnetic TIs of Cr-doped  $(\text{Bi}, \text{Sb})_2\text{Te}_3$ , where the  $C = 1$  has been reached [17]. The search for a QAH insulator with higher Chern numbers could be important both for fundamental and practical interests. The edge channels of the QAH insulator have been proposed as interconnects for integrated circuits [18]. However, while the edge channels of the QAH insulator conduct without dissipation, contact resistance could still limit possible applications in interconnects. The QAH effect with higher plateaus lowers the contact resistance, significantly improving the performance of the interconnect devices. Fractional filling of Chern insulators with  $C = 2$  could also lead to new topological states with novel elementary excitations [19]. The QAH effect with higher plateaus also shows a dramatic difference between the IQHE and the QAH effect: whereas a higher magnetic field leads to lower Hall conductance plateaus in the IQHE, a higher magnetic

moment leads to higher Hall conductance plateaus in the QAH effect.

In this Letter, we present a general theory for the QAH effect with higher plateaus. Based on the first-principles calculations, we predict that thin films of Cr-doped  $\text{Bi}_2(\text{Se}_x\text{Te}_{1-x})_3$  TIs are a candidate for the  $C = 2$  QAH insulator. The tunable magnetic ordering and SOC in this system provide an ideal platform for realizing other exotic topological states in magnetic TIs.

The basic mechanism for the quantum spin Hall effect or TI is the band inversion of spin degenerate bands, described by the Bernevig-Hughes-Zhang model [20]. Similarly, the basic mechanism for the QAH effect is the band inversion of spin polarized bands in magnetic TIs [5–9]. The general theory for the higher Chern number QAH effect presented in this Letter is generic for any thin films of magnetic TIs. We would like to start from a simple model describing the TIs  $\text{Bi}_2\text{Te}_3$ ,  $\text{Bi}_2\text{Se}_3$ , and  $\text{Sb}_2\text{Te}_3$  for concreteness [21]. The thin films made out of this family of compounds doped with Cr or Fe develop ferromagnetism even up to 190 K [22–24]. The QAH effect can be realized in a 2D thin film of such magnetic TIs with spontaneous FM order. The low-energy bands of these materials consist of a bonding and an antibonding state of  $p_z$  orbitals, labeled by  $|P2_z^-, \uparrow(\downarrow)\rangle$  and  $|P1_z^+, \uparrow(\downarrow)\rangle$ , respectively. The generic form of the effective Hamiltonian describing these four bands is

$$\mathcal{H}_{3\text{D}}(k_x, k_y, k_z) = \begin{pmatrix} H_+(k) & A_1 k_z i \sigma_y \\ -A_1 k_z i \sigma_y & H_-(k) \end{pmatrix}, \quad (1)$$

$$H_{\pm}(k) = \varepsilon(k) + d_{\pm}^i(k) \tau_i; \quad (2)$$

here,  $\tau_i$  ( $i = 1, 2, 3$ ) and  $\sigma_y$  are Pauli matrices, and  $d_{\pm}^{1,2,3}(k) = (A_2 k_x, \pm A_2 k_y, M(k) \mp \Delta)$ . To the lowest order in  $k$ ,  $M(k) = B_0 + B_1 k_x^2 + B_2 (k_x^2 + k_y^2)$  and  $\varepsilon(k) = D_0 + D_1 k_x^2 + D_2 (k_x^2 + k_y^2)$  account for the particle-hole asymmetry.  $B_0 < 0$  and  $B_1, B_2 > 0$  guarantee that the system is in the inverted regime. The basis of Eq. (1) is  $|P1_z^+, \uparrow\rangle$ ,

$|P2_z^-, \downarrow\rangle$ ,  $|P1_z^+, \downarrow\rangle$ , and  $|P2_z^-, \uparrow\rangle$ ; the  $\pm$  in the basis stand for the even and odd parity; and  $\uparrow$ ,  $\downarrow$  represent spin-up and down states, respectively.  $\Delta$  is the exchange field along the  $z$  axis introduced by the FM ordering. For simplicity, the same effective  $g$  factor for the two orbitals  $P1_z^+$  and  $P2_z^-$  is assumed.

The confinement of thin films of three-dimensional (3D) magnetic TIs in the  $z$  direction quantizes the momentum on this axis and leads to 2D subbands labeled by the subband index  $n$ . In order to illustrate the underlying physics clearly, we first take the limit  $A_1 = 0$ , in which case the system is decoupled into two classes of 2D models  $h_+(n)$  and  $h_-(n)$  with opposite chirality

$$\tilde{\mathcal{H}}_{2D}(n) = \begin{pmatrix} h_+(n) & 0 \\ 0 & h_-(n) \end{pmatrix}, \quad (3)$$

where  $h_{\pm}(n) = \tilde{\epsilon}_n 1_{2 \times 2} + (\tilde{M}_n \mp \Delta)\tau_3 + A_2 k_x \tau_1 \pm A_2 k_y \tau_2$ , expressed in the subspace of  $|E_n, \uparrow\rangle = \varphi_n(z)|P1_z^+, \uparrow\rangle$  and  $|H_n, \downarrow\rangle = \varphi_n(z)|P2_z^-, \downarrow\rangle$  for  $h_+(n)$  and  $|E_n, \downarrow\rangle = \varphi_n(z)|P1_z^+, \downarrow\rangle$  and  $|H_n, \uparrow\rangle = \varphi_n(z)|P2_z^-, \uparrow\rangle$  for  $h_-(n)$ .  $\tilde{\epsilon}_n = D_0 + D_1 \langle k_z^2 \rangle_n + D_2 (k_x^2 + k_y^2)$ ,  $\tilde{M}_n = B_0 + B_1 \langle k_z^2 \rangle_n + B_2 (k_x^2 + k_y^2)$ , and the confinement in a thin film of thickness  $d$  is given by the relation  $\varphi_n(z) = \sqrt{2/d} \sin(n\pi z/d + n\pi/2)$  and  $\langle k_z^2 \rangle_n = (n\pi/d)^2$  for subbands with the index  $n$ .  $|E_n, \uparrow \setminus \downarrow\rangle$  and  $|H_n, \uparrow \setminus \downarrow\rangle$  have parity  $(-1)^{n+1}$  and  $(-1)^n$ , respectively. At half filling, the effective models  $h_{\pm}(n)$  have a Chern number  $\pm 1$  or 0, depending on whether the Dirac mass is inverted ( $\tilde{M}_n \mp \Delta < 0$ ) or not ( $\tilde{M}_n \mp \Delta > 0$ ) at the  $\Gamma$  point. Thus, the total Chern number of the system is

$$C = N_+ - N_-, \quad (4)$$

where  $N_{\pm}$  is the number of  $h_{\pm}(n)$  with inverted Dirac mass, respectively. As shown in Fig. 1(a), when  $\Delta = 0$ ,  $N_+ = N_-$ ; thus, the net Hall conductance of this system vanishes, while the  $Z_2$  index  $N_+ \pmod{2}$  can be still non-zero, which gives the crossover from a 3D TI to a quantum spin Hall insulator [25]. When  $\Delta \neq 0$ ,  $N_+$  can be different from  $N_-$ . In the  $\Delta = \Delta_1$  case, only the Dirac mass of  $h_+(1)$  is inverted, and thus  $N_+ = 1$  and  $N_- = 0$ ; the system is in a QAH state with  $C = 1$ . When the exchange field is larger with  $\Delta = \Delta_2$  and the Dirac masses of  $h_+(1)$  and  $h_+(2)$  are inverted,  $N_+ = 2$  and  $N_- = 0$  give the QAH phase with  $C = 2$ .

With the criteria for the Chern number in Eq. (4), we can identify a phase diagram in the parameter space  $(\Delta, d)$ , as shown in Fig. 2, where we adopt the parameters of  $\text{Bi}_2(\text{Se}_{0.4}\text{Te}_{0.6})_3$  [21] and neglect the particle-hole-asymmetric term  $\tilde{\epsilon}_n$ , for it does not change the condition for band inversion. In the absence of the  $A_1$  term, the condition for the band inversion of  $h_{\pm}(n)$  is  $d > n\pi\sqrt{B_1/(\pm\Delta - B_0)}$ ; thus, the phase boundaries are given by  $d = n\pi\sqrt{B_1/(\pm\Delta - B_0)}$  [Fig. 2(a)]. The different QAH phases are denoted by the corresponding Chern numbers.

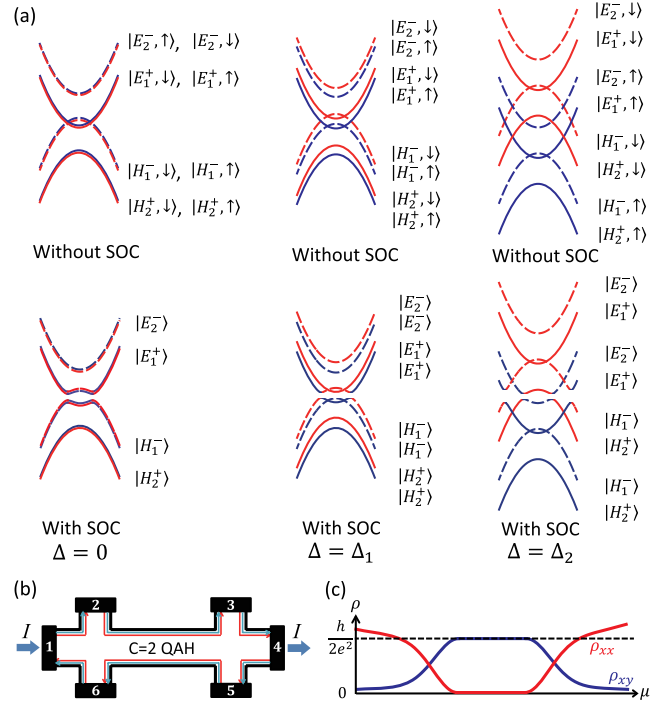


FIG. 1 (color online). Evolution of the subband structure upon increasing the exchange field. The solid lines denote the subbands that have even parity at the  $\Gamma$  point, and dashed lines denote subbands with odd parity at the  $\Gamma$  point. The blue color ( $\uparrow$ ) denotes the spin-up electrons, while red ( $\downarrow$ ) denotes spin-down electrons. The superscript + and - represent even and odd parity, respectively. (a) The initial  $(E_1, H_1)$  subbands are already inverted, while the  $(E_2, H_2)$  subbands are not inverted. The exchange field  $\Delta_1$  releases the band inversion in one pair of  $(E_1, H_1)$  subbands and increases the band inversion in the other pair, while the  $(E_2, H_2)$  subbands are still not inverted. With a stronger exchange field  $\Delta_2$ , a pair of inverted  $(E_2, H_2)$  subbands appears, while keeping only one pair of  $(E_1, H_1)$  subbands inverted. (b) Schematic drawing of a Hall bar device of the  $C = 2$  QAH effect. (c) Expected chemical potential dependence of zero magnetic field  $\rho_{xx}$  (in red) and  $\rho_{xy}$  (in blue).

As shown in Fig. 2(b), when the  $A_1$  term is turned on, it induces the coupling between  $h_{\pm}(n)$  and  $h_{\mp}(n+1)$ , which makes the QAH phases with the same Chern numbers simply connected in the phase diagram. Also, it enlarges the  $C = 1$  phase and shrinks the  $C = 2$  phase in the parameter space. The phase space of odd Chern number phases is simply connected, while those of even Chern number phases are separated into “islands,” for the confinement potential has inversion symmetry along the  $z$  direction.

For a given thickness, the Hall conductance experiences incremental plateaus  $0, e^2/h, 2e^2/h, \dots$ , as  $\Delta$  increases. Remarkably, the inverse of the magnetization, proportional to  $1/\Delta$  in the QAH effect, is analogous to the magnetic field in the IQHE. One the other hand, for a given exchange field, when the thickness  $d$  is small enough, the band inversion in the bulk band structure will be removed

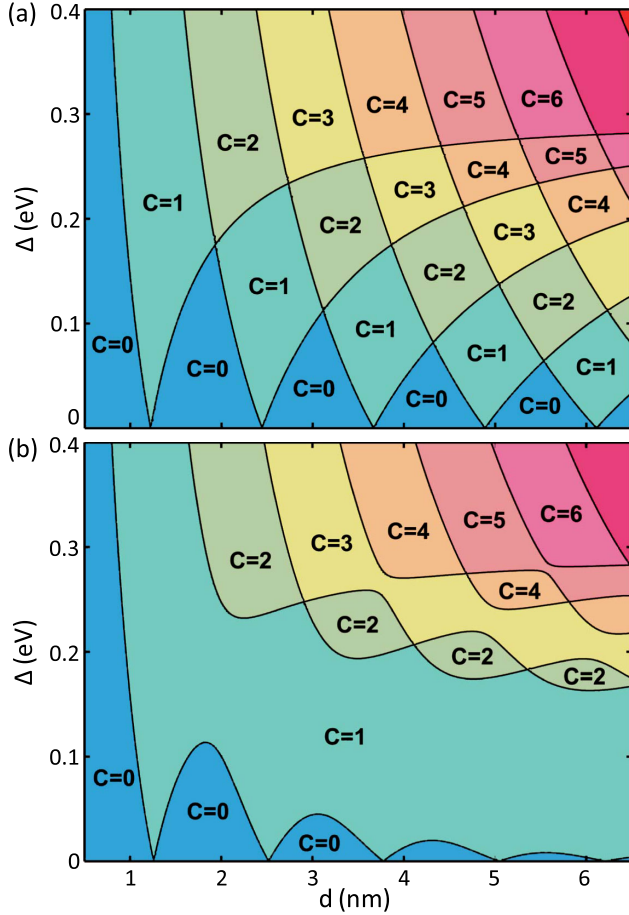


FIG. 2 (color online). The phase diagram of the QAH effect in thin films of magnetic TIs with two variables: the exchange field  $\Delta$  and thickness of thin film  $d$ . All parameters are taken from Ref. [21] for  $\text{Bi}_2(\text{Se}_{0.4}\text{Te}_{0.6})_3$ . (a),(b) Phase diagrams without and with the  $A_1$  term, respectively. The different QAH phases are denoted by corresponding Chern numbers. The particle-hole-asymmetric term is neglected, for it does not change the topology of the phase diagram. The width of each Hall plateau in the QAH effect depends on the band parameters and the thickness of the material, which is distinct from that in the IQHE.

entirely by the finite size effect; with the increasing  $d$ , the finite size effect is getting weaker and the band inversion among these subbands restores. If  $\Delta > |B_0|$ , the Dirac mass of class  $h_-(n)$  can never be inverted, and the Hall conductance plateau transition always increases as  $d$  increases. If  $\Delta$  is small, the Dirac mass of both classes can be inverted, and the system can only oscillate between a  $C = 1$  QAH insulator and a trivial band insulator as a function of thickness. Therefore, the QAH effect with higher plateaus requires a large enough exchange field.

The above discussion based on the analytic model gives us a clear physical picture of the high Chern number QAH effect in magnetic TIs. In the following, we would like to consider the possible realization in the realistic magnetic TI materials. The key point is to invert more spin polarized 2D subbands by a large exchange field, while keeping the

system full insulating. Thus, the SOC of the materials has to be properly tuned to keep a full band gap. For the Cr-doped  $(\text{Bi}, \text{Sb})_2\text{Te}_3$  magnetic TI used in experiment [17] to realize the  $C = 1$  QAH effect, the SOC of Te is so large that the  $C = 2$  QAH phase in this material becomes semimetallic.

We study the materials of  $\text{Bi}_{2-y}\text{Cr}_y(\text{Se}_x\text{Te}_{1-x})_3$  magnetic TIs. With different Cr content and the Se/Te ratio, the magnetic properties and SOC can be fine-tuned. We choose Cr-doped  $\text{Bi}_2(\text{Se}_{0.4}\text{Te}_{0.6})_3$  as an example, where the Dirac cone of surface states is observed to locate in the bulk band gap [26]. Here, we first carried out the first-principles calculations on 3D  $\text{Bi}_2(\text{Se}_{0.4}\text{Te}_{0.6})_3$  without SOC; the virtual crystal approximation is employed to simulate the mixing between Se and Te in first-principles calculations. Then, we get the effective SOC parameter of  $\text{Bi}_{2-y}\text{Cr}_y$  by fitting the band structure of  $\text{Bi}_{1.78}\text{Cr}_{0.22}(\text{Se}_{0.6}\text{Te}_{0.4})_3$  in Ref. [26]. This system is at the critical point of the topological phase transition from inverted bands to normal bands because the substitution of Bi by Cr reduces SOC strength. Finally, we construct the tight-binding model with SOC and the exchange interaction based on maximally localized Wannier functions [27,28]. When the 2D system stays in the QAH phase, there are topologically protected chiral edge states at the 1D edge. To show the topological feature more explicitly, we calculate the dispersion spectra of the chiral edge states directly. As examples, here we study the edge states of the 6 quintuple layers (QLs) and 12 QLs of  $\text{Bi}_{2-y}\text{Cr}_y(\text{Se}_{0.4}\text{Te}_{0.6})_3$  film along the  $[1\bar{1}]$  direction (edge A along  $\Gamma$ -M), as shown in Fig. 3. Each QL is about 1 nm thick. For a semi-infinite system, combining the tight-binding model with the iterative method [29], we can calculate the Green's function for the edge states directly. The local density of states (LDOS) is directly related to the imaginary part of the Green's function, from which we can obtain the dispersion of the edge states. As shown in Fig. 3(f) for 12 QLs  $\text{Bi}_{1.78}\text{Cr}_{0.22}(\text{Se}_{0.4}\text{Te}_{0.6})_3$  with  $\Delta = 0.14$  eV, there indeed exist two gapless chiral edge states  $\Sigma_1$  and  $\Sigma_2$  in the 2D bulk gap, indicating the  $C = 2$  QAH effect.

Recent experiments have shown that the thickness of thin film TIs can be well controlled through layer-by-layer growth via molecular beam epitaxy [30], and the exchange field  $\Delta$  can be tuned by changing the doping concentration  $y$  of the magnetic elements [22–24]. In the mean field approximation,  $\Delta$  can be estimated as  $\Delta = yJ_{\text{eff}}\langle S \rangle/2$ , where  $\langle S \rangle$  is the mean field expectation value of the local spin, and  $J_{\text{eff}}$  is the effective exchange parameter between local moments and the band electron. For Cr-doped  $\text{Bi}_2(\text{Se}, \text{Te})_3$ ,  $\langle S \rangle = 3/2$ ,  $J_{\text{eff}}$  is around 2.7 eV [9], and the FM Curie temperature is about tens of K. With the concentration of the magnetic dopants to be 10%, the exchange field can be as large as 0.2 eV, making the realization of a QAH effect with higher plateaus feasible.

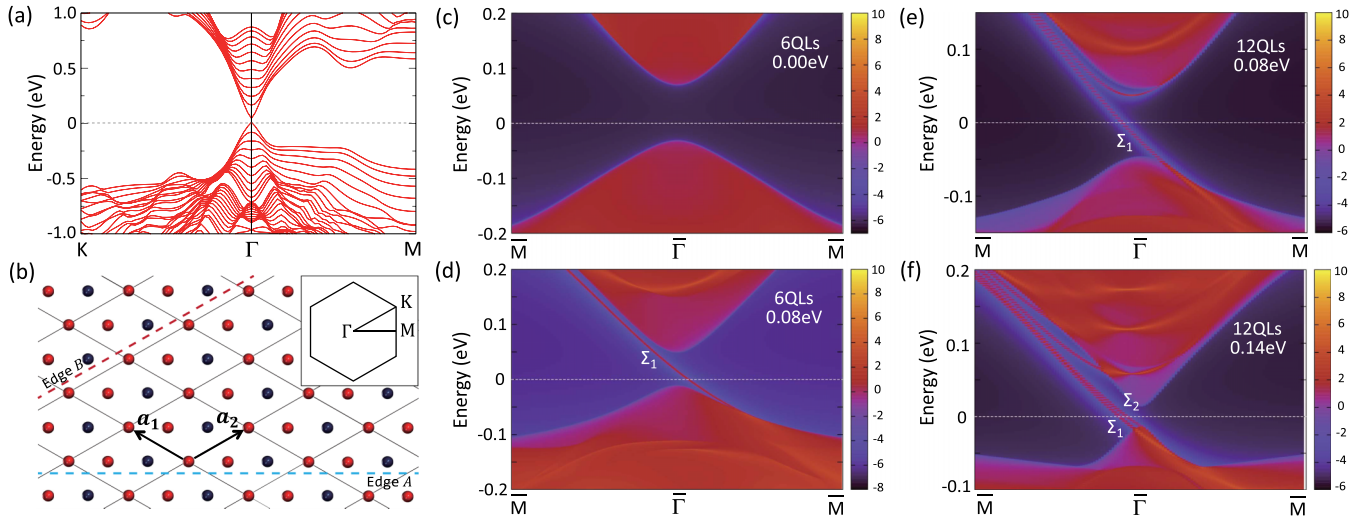


FIG. 3 (color online). Band structure, Brillouin zone, and edge states. (a) Band structure for 12 QLs  $\text{Bi}_{1.78}\text{Cr}_{0.22}(\text{Se}_{0.4}\text{Te}_{0.6})_3$  without an exchange field. The dashed line indicates the Fermi level. (b) The top view of a 2D thin film with two in-plane lattice vectors  $\mathbf{a}_1$  and  $\mathbf{a}_2$ . The 1D edges are indicated by the dashed lines, edge A along the  $[1\bar{1}]$  direction and edge B along the  $[01]$  direction. The inset shows the 2D Brillouin zone, in which the high-symmetry  $\mathbf{k}$  points  $\Gamma(0,0)$ ,  $K(\pi,\pi)$ , and  $M(\pi,0)$  are labeled. (c)–(f) Energy and momentum dependence of the LDOS along edge A for the  $\text{Bi}_{1.78}\text{Cr}_{0.22}(\text{Se}_{0.4}\text{Te}_{0.6})_3$  film with a thickness of 6 QLs and an exchange field of (c) 0.0 eV and (d) 0.08 eV and with a thickness of 12 QLs and an exchange field of (e) 0.08 eV and (f) 0.14 eV. Here, the warmer colors (lighter gray in gray scale) represent a higher LDOS. The red (light gray) and blue (dark gray) regions indicate 2D bulk energy bands and energy gaps, respectively. The gapless chiral edge states can be clearly seen around the  $\Gamma$  point as red (light gray) lines dispersing in the 2D bulk gap. In (c)–(f), the number of chiral edge states is  $C = 0,1,1,2$ .

Experimentally, for the QAH effect with a higher Chern number  $C$ , the gate-tuned Hall resistance  $\rho_{xy}$  should be accurately quantized into the  $h/Ce^2$  plateau at zero magnetic field accompanied by a vanishing longitudinal resistance  $\rho_{xx}$  and conductance, as shown in Fig. 1(c). In real materials, there always exist residual dissipative conduction channels contributed by a small amount of bulk carriers; however, if the carrier density is low enough, they will become localized states by the disorder potentials and will not affect the exact quantization of the Hall plateau.

The dissipationless chiral edge channels of the QAH insulator are ideal for interconnect applications [18]. As no dissipation occurs along the edge channel itself, the only resistance is the contact resistance. For the QAH insulators with high Chern number  $C$ , the contact resistance is  $h/Ce^2$  (the length of the sample can be as large as several hundreds of  $\mu\text{m}$  [17]). Compared with the commercially used copper interconnect, for the width of copper wire is 10 nm, the resistance of the copper interconnect is  $8 \times 10^3 \Omega/\mu\text{m}$  times the length  $L$  [31]. The contact resistance of the  $C = 2$  QAH insulator will be smaller than the copper interconnect when the length exceeds 1.5  $\mu\text{m}$ .

The QAH effect with higher plateaus may provide a setting for both fundamental and applied investigations. A wealth of materials with tunable magnetic and topological properties [32,33] could lead to the discovery of more high Chern number QAH insulators [34]. The multiple dissipationless edge channels in the higher plateau QAH effect would offer better ways to optimize electrical

transport properties, leading to novel designs for low-power-consumption electronics.

We are grateful to X. L. Qi for insightful discussions. This work is supported by the Defense Advanced Research Projects Agency Microsystems Technology Office, MesoDynamic Architecture Program (MESO), through Contract No. N66001-11-1-4105, the DARPA Program on “Topological Insulators—Solid State Chemistry, New Materials and Properties,” under Grant No. N66001-12-1-4034, and by the U.S. Department of Energy, Office of Basic Energy Sciences, Division of Materials Sciences and Engineering, under Contract No. DE-AC02-76SF00515.

- 
- [1] D. J. Thouless, M. Kohmoto, M. P. Nightingale, and M. den Nijs, *Phys. Rev. Lett.* **49**, 405 (1982).
  - [2] K. v. Klitzing, G. Dorda, and M. Pepper, *Phys. Rev. Lett.* **45**, 494 (1980).
  - [3] B. I. Halperin, *Phys. Rev. B* **25**, 2185 (1982).
  - [4] F. D. M. Haldane, *Phys. Rev. Lett.* **61**, 2015 (1988).
  - [5] X.-L. Qi, Y.-S. Wu, and S.-C. Zhang, *Phys. Rev. B* **74**, 085308 (2006).
  - [6] X.-L. Qi, T. L. Hughes, and S.-C. Zhang, *Phys. Rev. B* **78**, 195424 (2008).
  - [7] C.-X. Liu, X.-L. Qi, X. Dai, Z. Fang, and S.-C. Zhang, *Phys. Rev. Lett.* **101**, 146802 (2008).
  - [8] R. Li, J. Wang, X. L. Qi, and S. C. Zhang, *Nat. Phys.* **6**, 284 (2010).
  - [9] R. Yu, W. Zhang, H.-J. Zhang, S.-C. Zhang, X. Dai, and Z. Fang, *Science* **329**, 61 (2010).

- [10] H. Jiang, Z. Qiao, H. Liu, and Q. Niu, *Phys. Rev. B* **85**, 045445 (2012).
- [11] D. Xiao, W. Zhu, Y. Ran, N. Nagaosa, and S. Okamoto, *Nat. Commun.* **2**, 596 (2011).
- [12] A. Rüegg and G. A. Fiete, *Phys. Rev. B* **84**, 201103 (2011).
- [13] K.-Y. Yang, W. Zhu, D. Xiao, S. Okamoto, Z. Wang, and Y. Ran, *Phys. Rev. B* **84**, 201104 (2011).
- [14] F. Wang and Y. Ran, *Phys. Rev. B* **84**, 241103 (2011).
- [15] X. Hu, A. Rüegg, and G. A. Fiete, *Phys. Rev. B* **86**, 235141 (2012).
- [16] A. Rüegg, C. Mitra, A. A. Demkov, and G. A. Fiete, *Phys. Rev. B* **85**, 245131 (2012).
- [17] C.-Z. Chang, J. Zhang, X. Feng, J. Shen, Z. Zhang, M. Guo, K. Li, Y. Ou, P. Wei, L.-L. Wang, Z.-Q. Ji, Y. Feng, S. Ji, X. Chen, J. Jia, X. Dai, Z. Fang, S.-C. Zhang, K. He, Y. Wang, L. Lu, X.-C. Ma, and Q.-K. Xue, *Science* **340**, 167 (2013).
- [18] X. Zhang and S.-C. Zhang, *Proc. SPIE Int. Soc. Opt. Eng.* **8373**, 837309 (2012).
- [19] M. Barkeshli and X.-L. Qi, *Phys. Rev. X* **2**, 031013 (2012).
- [20] B. A. Bernevig, T. L. Hughes, and S. C. Zhang, *Science* **314**, 1757 (2006).
- [21] H. Zhang, C.-X. Liu, X.-L. Qi, X. Dai, Z. Fang, and S.-C. Zhang, *Nat. Phys.* **5**, 438 (2009).
- [22] V. Kul'bachinskii, A. Kaminskii, K. Kindo, Y. Narumi, K. Suga, P. Lostak, and P. Svanda, *Pis'ma Zh. Eksp. Teor. Fiz.* **73**, 396 (2001); [*JETP Lett.* **73**, 352 (2001)].
- [23] Z. Zhou, Y.-J. Chien, and C. Uher, *Phys. Rev. B* **74**, 224418 (2006).
- [24] C.-Z. Chang, J. Zhang, M. Liu, Z. Zhang, X. Feng, K. Li, L.-L. Wang, X. Chen, X. Dai, Z. Fang, X.-L. Qi, S.-C. Zhang, Y. Wang, K. He, X.-C. Ma, and Q.-K. Xue, *Adv. Mater.* **25**, 1065 (2013).
- [25] C.-X. Liu, H. J. Zhang, B. Yan, X.-L. Qi, T. Frauenheim, X. Dai, Z. Fang, and S.-C. Zhang, *Phys. Rev. B* **81**, 041307 (2010).
- [26] J. Zhang, C.-Z. Chang, P. Tang, Z. Zhang, X. Feng, K. Li, L.-L. Wang, X. Chen, C. Liu, W. Duan, K. He, Q.-K. Xue, X. Ma, and Y. Wang, *Science* **339**, 1582 (2013).
- [27] N. Marzari and D. Vanderbilt, *Phys. Rev. B* **56**, 12847 (1997).
- [28] I. Souza, N. Marzari, and D. Vanderbilt, *Phys. Rev. B* **65**, 035109 (2001).
- [29] M. P. L. Sancho, J. M. L. Sancho, and J. Rubio, *J. Phys. F* **14**, 1205 (1984).
- [30] Y. Zhang, K. He, C.-Z. Chang, C.-L. Song, L.-L. Wang, X. Chen, J.-F. Jia, Z. Fang, X. Dai, W.-Y. Shan, S.-Q. Shen, Q. Niu, X.-L. Qi, S.-C. Zhang, X.-C. Ma, and Q.-K. Xue, *Nat. Phys.* **6**, 584 (2010).
- [31] A. Naeemi and J. D. Meindl, *IEEE Electron Device Lett.* **28**, 428 (2007).
- [32] S.-Y. Xu, Y. Xia, L. A. Wray, S. Jia, F. Meier, J. H. Dil, J. Osterwalder, B. Slomski, A. Bansil, H. Lin, R. J. Cava, and M. Z. Hasan, *Science* **332**, 560 (2011).
- [33] M. Brahlek, N. Bansal, N. Koirala, S.-Y. Xu, M. Neupane, C. Liu, M. Z. Hasan, and S. Oh, *Phys. Rev. Lett.* **109**, 186403 (2012).
- [34] C. Fang, M. J. Gilbert, and B. A. Bernevig, [arXiv:1306.0888](https://arxiv.org/abs/1306.0888).